Journal of Power Sources 194 (2009) 786–793

Contents lists available at ScienceDirect

Journal of Power Sources

journal homepage: www.elsevier.com/locate/jpowsour

Synthesis of $LiFe_{1-x}Ni_xPO_4$/C composites and their electrochemical performance

Yang Lu [a], Jichen Shi [a], Zaiping Guo [b,c], Qingsong Tong [a,*], Weijing Huang [a], Bianyun Li [a]

[a] College of Chemistry and Materials Science, Fujian Normal University, Fujian, Fuzhou 350007, China
[b] Institute for Superconducting & Electronic Materials, University of Wollongong, NSW 2522, Australia
[c] School of Mechanical, Materials & Mechatronic Engineering, University of Wollongong, NSW 2522, Australia

ARTICLE INFO

Article history:
Received 5 April 2009
Received in revised form 21 May 2009
Accepted 22 May 2009
Available online 30 May 2009

Keywords:
Lithium iron phosphate
Nickel doping
Cycling performance
Electrochemical impedance spectra

ABSTRACT

$LiFePO_4$/C and $LiFe_{1-x}Ni_xPO_4$/C ($x = 0$, 0.02, 0.04, and 0.06) composites were prepared using solid-state reaction. The as-prepared composites were characterized by using X-ray diffraction, charge–discharge cycling, cyclic voltammograms, Raman spectroscopy, field emission scanning electron microscopy, high-resolution transmission electron microscopy, and other techniques. The experimental results show that all as-prepared composites have a single phase of orthorhombic olivine-type structure with the *Pnmb* space group. The as-prepared $LiFe_{1-x}Ni_xPO_4$/C composites exhibit high capacities and good cycling performance; e.g., the $LiFe_{0.98}Ni_{0.02}PO_4$/C composite delivers 142 and 138 mAh g^{-1} at the 0.1 C rate for the first and fifth cycles, respectively. Such composites also show good rate capabilities; e.g., when discharged at the 2 C rate the $LiFe_{0.98}Ni_{0.02}PO_4$/C composite delivers an initial capacity of 121 mAh g^{-1}, 85% of the discharge capacity at the 0.1 C rate. The reason why the $LiFe_{1-x}Ni_xPO_4$/C composites have better electrochemical performance compared to the $LiFePO_4$/C composites is because nickel doping enhances the P—O bond, stabilizes the structure, and thus the charge-transfer resistance and cathode particle resistance of the composites are decreased.

1. Introduction

Since $LiFePO_4$ was identified as a promising cathode material for lithium-ion batteries by Goodenough and co-workers in 1997 [1], numerous researchers have engaged in the investigation of $LiFePO_4$ based materials [2,3] because of their low cost, environmental friendliness, cheap and abundant raw materials, excellent thermal stability, safety characteristics, good electrochemical performance, and high theoretical specific capacity (170 mAh g^{-1}), with a long voltage plateau on the discharge curves [4]. The key barrier to commercialization of $LiFePO_4$ has been its low electronic and ionic conductivities [5,6]. In order to solve this problem with $LiFePO_4$, reducing the particle size, effectively coating carbon on the surface, and doping cations into the structure of the $LiFePO_4$ have been widely studied by many researchers over the past few years [7–10]. Reducing the particle size benefits lithium ion insertion/extraction, which consequently helps improve the ionic conductivity of $LiFePO_4$; by contrast, coating with carbon helps to modify the total electronic conductivity of $LiFePO_4$/C composites, while doping with cations may improve the intrinsic electronic conductivity of $LiFePO_4$ materials. Carbon coating has been investigated extensively by using various organic precursors or by different coating approaches. However, the carbon cannot increase the intrinsic electronic or ionic conductivity of $LiFePO_4$. In addition, the excess carbon in $LiFePO_4$ decreases the specific volume capacity of the composite. Therefore, doping with cations (such as Co^{2+} [11], Cr^{3+} [12], Ti^{4+} [13], V^{5+} [14], Al^{3+} [15], and Mg^{2+} [16]) has been introduced to modify the electrochemical performance of $LiFePO_4$ materials. For example, compared to the pristine $LiFePO_4$, a cobalt doped sample was found to have less covalent of P—O bonds due to the increased covalence of Fe^{3+}—O bonds via the inductive effect. Note that the bond energy (ΔH_{f298}) of Ni—O (391.6 kJ mol^{-1}) is larger than that of Co—O (368 kJ mol^{-1}) and smaller than that of Fe—O (409 kJ mol^{-1}) [17]. Meanwhile, the sizes of Ni^{2+} ions ($r_{Ni}{}^{2+}$) for coordination numbers of 4 and 6, 0.055 and 0.069 Å, are larger than those of Co^{2+} ions (i.e., 0.038 and 0.065 Å for coordination numbers of 4 and 6, respectively) [17]. Therefore, compared to Co—O bonds, the Ni—O bonds with longer bond length are more stable. It is likely that nickel ion doping could stabilize the covalent of P—O bonds in $LiFePO_4$, similarly to what happens in cobalt doped samples [11]. In this study, we introduce doping with nickel ions into the structure of $LiFePO_4$ material to improve its electrochemical performance.

2. Experimental

2.1. Sample preparation

$LiFePO_4$/C composites were prepared by a mechano-chemical activation method as described below: $NH_4H_2PO_4$ (Aldrich), Li_2CO_3 (Aldrich), and $FeC_2O_4{\cdot}2H_2O$ (Aldrich) were mixed according to

* Corresponding author. Tel.: +86 591 83530270; fax: +86 591 83530270.
E-mail address: qstong_3503@fjnu.edu.cn (Q. Tong).

0378-7753/$ – see front matter.
doi:10.1016/j.jpowsour.2009.05.041

the molar ratio of Li:Fe:PO_4 = 1:1:1. The mixture was subsequently mixed with some glucose to carbon coat the particles in the weight ratio of 95:5, and it was then ball milled in a planetary mill for 2 h (with ethyl alcohol as a liquid medium). The resulting precursor was dried at 90 °C for 5 h in a vacuum dryer, and then sintered in a tube furnace under flowing argon at 660, 720, and 780 °C, to yield samples $LiFePO_4$/C-660, $LiFePO_4$/C-720, and $LiFePO_4$/C-780, respectively. The as-prepared composites were removed from the furnace after cooling down to room temperature.

$LiFe_{1-x}Ni_xPO_4$/C (x = 0, 0.02, 0.04, and 0.06) composites were prepared by the same processes as described above, but with $Ni(OH)_2$ (Aldrich) substituting for a part of the $FeC_2O_4{\cdot}2H_2O$ according to the molar ratio of Fe:Ni = $(1-x)$:x, x = 0, 0.02, 0.04, and 0.06. Note that the sintering temperature for the nickel doped composites is the optimized one for the un-doped composite (i.e., 720 °C).

2.2. Crystal structure of the samples

The phase identification of the as-prepared composites was conducted by using X-ray diffraction (XRD) on a Philips X'pert MPD Pro (Netherlands) with Cu Kα radiation (λ = 1.54178 Å). The diffraction patterns were collected from a 10 to 90° 2θ angle at 40 kV and 40 mA with a scan step size of 0.02° and a step time of 0.3 s.

2.3. Charge–discharge performance of the samples

Fresh coin cells (R2025) were fabricated, consisting of a cathode, a lithium-metal anode, a Celgard 2400 separator, and LP30 electrolyte. The coin cells were assembled in an Ar-filled glove box [18]. The cathode was obtained from a mixture of 85 wt.% active materials, 10 wt.% carbon (Super S), and 5 wt.% polyvinylidene fluoride binder pasted onto aluminum foil. The pasted foil was handled as described in the literature [18]. The cells were flooded with 1 mol L^{-1} $LiPF_6$ dissolved in ethylene carbonate/methoxyethane in a 1:1 weight ratio (LP30, Merck Co.). The charge/discharge cycling was carried out on a Neware system in the voltage range of 4.2–2.5 V at the current densities of 15 mA g^{-1} (0.1 C rate), 150 mA g^{-1} (1 C rate), 300 mA g^{-1} (2 C rate), 1500 mA g^{-1} (10 C rate), and 4500 mA g^{-1} (30 C rate), respectively.

2.4. Cyclic voltammetry (CV) and electrochemical impedance spectroscopy (EIS) measurements

EIS and CV measurements were carried out on a CHI660C electrochemical workstation (Chenghua, China). During EIS measurements, the amplitude of the AC signal was 5 mV over the frequency range between 100 kHz and 0.01 Hz. During CV measurements, the curves were recorded between 4.4 and 1.9 V (vs. Li^+/Li) at the scan rates of 0.2, 0.4, 0.6, 0.8, and 1.0 mV s^{-1}, respectively, in a three-electrode cell. The working electrodes were fabricated as described in the literature [19,20] by drying a slurry, which was coated onto Al foil at 125 °C in a vacuum oven. Both the counter and the reference electrodes were lithium-metal foil. The three-electrode cell assembly was carried out in an Ar-filled glove box. The cells were flooded with 1 mol L^{-1} $LiPF_6$ dissolved in ethylene carbonate/methoxyethane in a 1:1 weight ratio (LP30, Merck Co.). The electrochemical measurements were started as soon as the three-electrode cell was immersed in electrolyte at room temperature.

2.5. Fourier transformed infrared spectroscopy (FTIR) and Raman spectroscopy measurements

FTIR spectra of the as-prepared composites were collected on a Nicolet Avatar 360 FTIR spectrometer. The final FTIR spectra were the average of 64 survey-scans with a resolution of 2 cm^{-1}. Raman spectra were collected on a confocal microprobe Raman system (Renishaw Invia Plus, England) with a 514 nm excitation line. The spectra were recorded with the average of three survey-scans and a resolution of 1 cm^{-1}.

2.6. Morphology of the samples

The morphology of the as-prepared composites was observed on a field emission scanning electron microscope (FESEM; JSM-7500F, Japan) operating at 20.0 kV. The transmission electron microscopy (TEM) observation was carried out on a high-resolution transmission electron microscopy (HRTEM, Tecnai G2 F20 S-TWIN, Japan) operating at 200 KV.

3. Results and discussion

3.1. Structural properties

Fig. 1 shows the X-ray diffraction (XRD) patterns of the as-prepared composites. All the peaks were indexed to a single phase of an orthorhombic olivine-type structure with space group *Pnmb*. No impurity peaks were observed in Fig. 1, indicating the high purity of the as-prepared composites.

The lattice parameters of the as-prepared composites were calculated based on the XRD patterns and are listed in Table 1. The unit cell of sample $LiFePO_4$/C-720 is slightly larger than those of $LiFePO_4$/C-660 and $LiFePO_4$/C-780, suggesting easier insertion and extraction of lithium ions in $LiFePO_4$/C-720 among the three un-

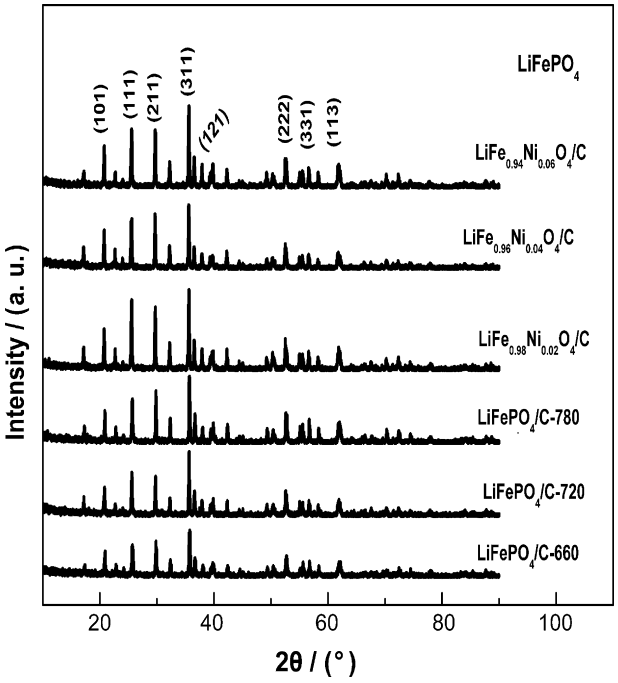

Fig. 1. XRD patterns of the as-prepared composites.

Table 1
Lattice parameters of the as-prepared composites.

Composite	a (Å)	b (Å)	c (Å)	V (Å^3)
$LiFePO_4$/C-660	10.21	6.00	4.67	287.0
$LiFePO_4$/C-720	10.30	6.00	4.68	289.4
$LiFePO_4$/C-780	10.26	6.00	4.68	288.1
$LiFe_{0.98}Ni_{0.02}PO_4$/C	10.30	6.01	4.69	290.9
$LiFe_{0.96}Ni_{0.04}PO_4$/C	10.35	6.02	4.70	292.4
$LiFe_{0.94}Ni_{0.06}PO_4$/C	10.30	6.02	4.69	291.0

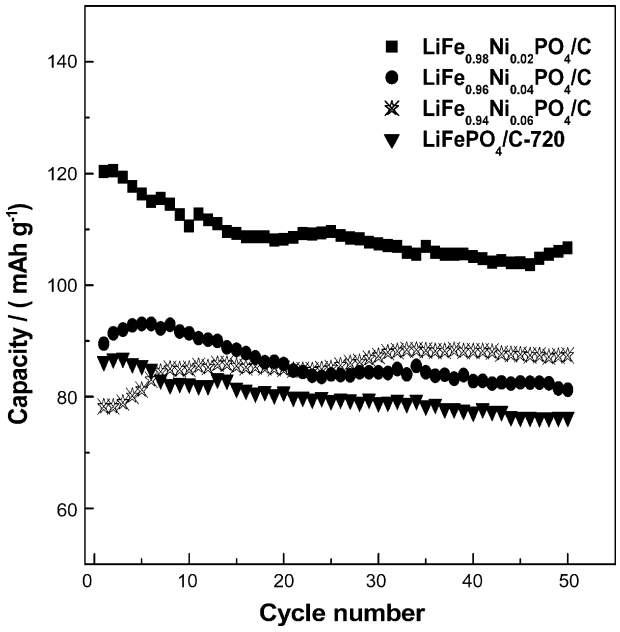

Fig. 2. The cycling performance of the nickel doped and un-doped composites at the 2 C rate (2.5–4.2 V).

doped materials. Comparison between the $LiFePO_4$/C-720 and the nickel doped composites suggests that the nickel dopant causes an expansion in the volume of the orthorhombic cell. Among the nickel doped composites, the $LiFe_{0.98}Ni_{0.02}PO_4$/C composite possesses the smallest cell, indicating that its lattice is the most stable. Nytén and Thomas [21] suggested that the $LiCo_{0.75}Fe_{0.25}PO_4$ composition has stronger M—O bonding because the mean M—O (M=Co, Fe) distance in the $LiCo_{0.75}Fe_{0.25}PO_4$ composite is slightly shorter than in other composites. Thus, we expect the $LiFe_{0.98}Ni_{0.02}PO_4$/C composite to have a more stable structure for the charge/discharge reaction, and consequently to have better cyclic performance.

3.2. Cycling performance of the as-prepared samples

Samples $LiFePO_4$/C-660, $LiFePO_4$/C-720, and $LiFePO_4$/C-780 were charged/discharged for 50 cycles at the 1 C rate, and their discharge capacities are 91, 114, and 100 mAh g^{-1} in the 1st cycle, and 94, 116, and 103 mAh g^{-1} in the 50th cycle, respectively (not shown). Therefore, the un-doped composite prepared at 720 °C ($LiFePO_4$/C-720) shows the best electrochemical performance among all the un-doped composites.

Fig. 2 shows the cycling performance at the 2 C rate of the nickel doped and un-doped composites prepared at 720 °C. The discharge capacities of the $LiFePO_4$/C-720, $LiFe_{0.98}Ni_{0.02}PO_4$/C, $LiFe_{0.96}Ni_{0.04}PO_4$/C, and $LiFe_{0.94}Ni_{0.06}PO_4$/C composites are 86, 121, 90, and 78 mAh g^{-1} in the 1st cycle, and 76, 108, 82, and 88 mAh g^{-1} in the 50th cycle, respectively. Comparison among the nickel doped and the un-doped composites indicates that the $LiFe_{0.98}Ni_{0.02}PO_4$/C composite shows the best electrochemical performance.

Fig. 3 shows the initial discharge curves of the $LiFePO_4$/C-720 composite, which has capacities of 86, 114, and 126 mAh g^{-1} at the 2 C, 1 C, and 0.1 C rates, respectively. The $LiFePO_4$/C-720 composite exhibits discharge plateaus at 3.25 V (53 mAh g^{-1}), 3.35 V (85 mAh g^{-1}), and 3.39 V (95 mAh g^{-1}) when discharged at the 2 C, 1 C, and 0.1 C rates, respectively; note here that the values in the parentheses refer to the capacities at the plateau potentials. Fig. 4 shows the initial discharge curves of the $LiFe_{0.98}Ni_{0.02}PO_4$/C composite, which has respective capacities of 35, 70, 121, 127, and 142 mAh g^{-1}, while discharged at the 30 C, 10 C, 2 C, 1 C, and 0.1 C rates in the voltage range of 4.2–2.5 V. Compared to the un-

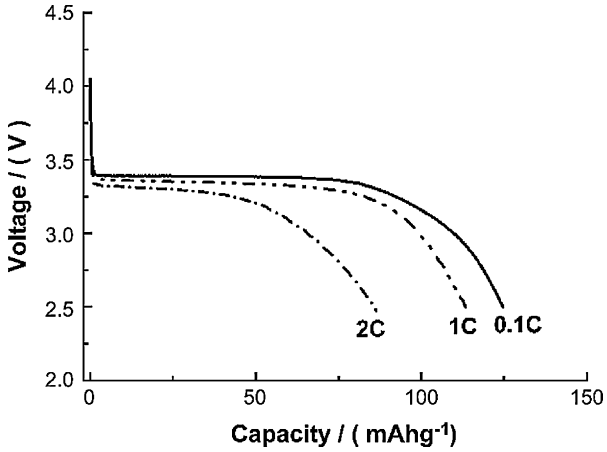

Fig. 3. Initial discharge curves of the $LiFePO_4$/C-720 composite discharged at different rates.

doped sample (Fig. 3), the $LiFe_{0.98}Ni_{0.02}PO_4$/C composite exhibits discharge plateaus at 3.11 V (20 mAh g^{-1}), 3.22 V (45 mAh g^{-1}), 3.29 V (87 mAh g^{-1}), 3.35 V (89 mAh g^{-1}), and 3.40 V (96 mAh g^{-1}) when discharged at the 30 C, 10 C, 2 C, 1 C, and 0.1 C rates, respectively (Fig. 4). After 50 cycles the discharge capacities of the $LiFe_{0.98}Ni_{0.02}PO_4$/C showed retained capacities of 35, 67, 108, 119, and 138 mAh g^{-1} for the 30 C, 10 C, 2 C, 1 C, and 0.1 C rates, respectively. The Fig. 4 discharge curves show that the discharge plateau of the $LiFe_{0.98}Ni_{0.02}PO_4$/C composite is flatter around 3.4 V than what is seen in Fig. 3. Therefore, the nickel dopant strongly improves the electrochemical performance of lithium iron phosphate, especially when the $LiFe_{0.98}Ni_{0.02}PO_4$/C composite was discharged at a high rate (e.g., 2 C).

Cobalt has also been reported to substitute into the structure of $LiFePO_4$ to modify its electrochemical performance; for examples, Wang et al. [22] prepared a $LiFe_{0.8}Co_{0.2}PO_4$ sample exhibits the initial capacity of 138 mAh g^{-1} and retained 88.4% of its initial value after 20 cycles at a current density of 10 mA g^{-1}, while Shanmukaraj et al. [23] found that $LiFe_{0.98}Co_{0.02}PO_4$/C delivered an initial capacity of 76 mAh g^{-1} at the 1 C rate. By contrast, nickel doped $LiFePO_4$ samples usually show better electrochemical cycling performance; for examples, Cheng et al. [24] found that $Li_{1-2x}Ni_xFePO_4$ had an initial capacity of 143.2 mAh g^{-1}, and its capacity fading was as high as 8.4% in 20 cycles at the 0.1 C rate, while Wang et al. [25] reported that $LiFe_{0.9}Ni_{0.1}PO_4$ had an initial capacity of 130 mAh g^{-1} at 0.2 C and 70 mAh g^{-1} at 10 C in the voltage range of 4.2–2.5 V.

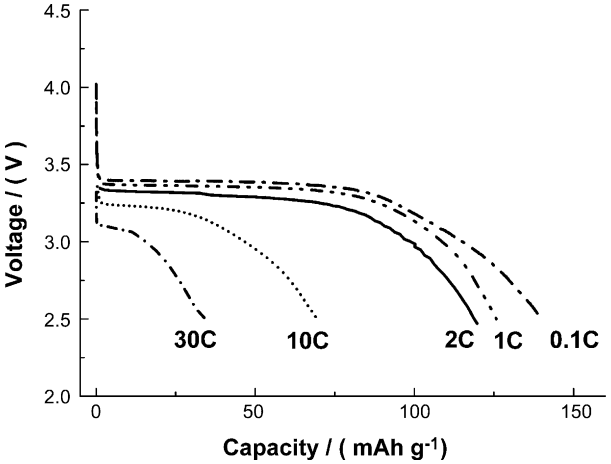

Fig. 4. Initial discharge curves of the $LiFe_{0.98}Ni_{0.02}PO_4$/C composite discharged at different rates.

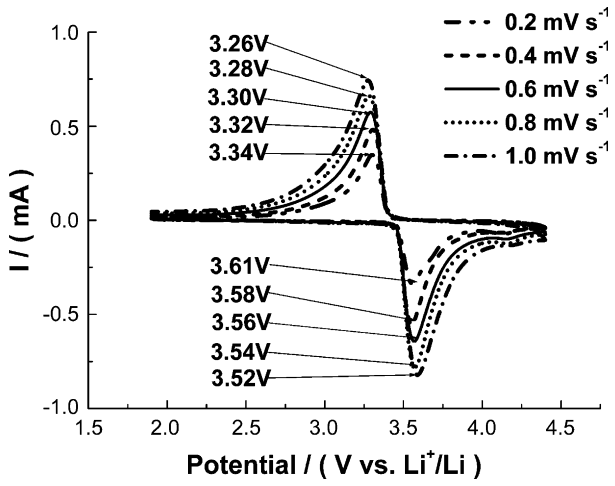

Fig. 5. Cyclic voltammograms of the $LiFe_{0.98}Ni_{0.02}PO_4$/C composites (scan rates: 0.2, 0.4, 0.6, 0.8 and 1.0 mV s^{-1}).

As a result, compared to the samples of Cheng et al. [24], Wang et al. [22,25], and Shanmukaraj et al. [23], our $LiFe_{0.98}Ni_{0.02}PO_4$/C composite shows better electrochemical performance; the reason is uncertain at the present stage; however, the doping level is possibly more appropriate for our sample.

3.3. Cyclic voltammograms of the samples

Fig. 5 shows cyclic voltammetry curves of the $LiFe_{0.98}Ni_{0.02}PO_4$ composite measured at the scan rates of 0.2, 0.4, 0.6, 0.8, and 1.0 mV s^{-1}, respectively. When the scan rate was 0.2 mV s^{-1}, the oxidation and main reduction peaks in the 1st cycle appeared at around 3.61 and 3.34 V, respectively; the potential interval between two peaks is 0.27 V. However, when the scan rate of the potential was 1.0 mV s^{-1}, the oxidation and main reduction peaks in the 1st cycle appeared at around 3.52 and 3.26 V, respectively: the potential interval between the two peaks is 0.26 V. The redox peak profile of the $LiFe_{0.98}Ni_{0.02}PO_4$ composite is more symmetric than that of pure $LiFePO_4$ or a composite of lithium iron phosphate and multi-wall carbon nanotubes ($LiFePO_4$-MWCNT) [26], demonstrating that the reversibility and reactivity of the $LiFe_{0.98}Ni_{0.02}PO_4$ composite are enhanced.

The linear relationship between the peak current (I_p) and the square root of the scan rate of the potential ($v^{1/2}$) for the $LiFe_{0.98}Ni_{0.02}PO_4$/C composite was calculated and is shown in Fig. 6. In a reversible system, the relationship between I_p and the Li ion

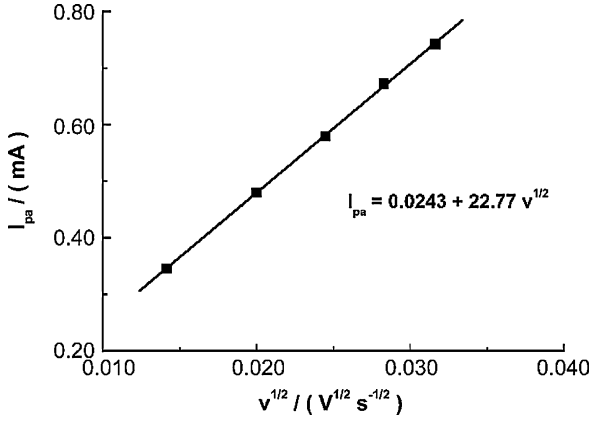

Fig. 6. Relationship between peak current (I_p) and the square root of the scan rate ($v^{1/2}$) for the $LiFe_{0.98}Ni_{0.02}PO_4$/C composite.

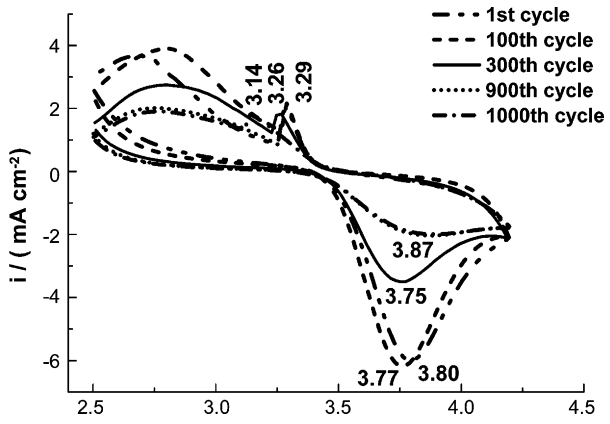

Fig. 7. Cyclic voltammograms of the $LiFe_{0.98}Ni_{0.02}PO_4$/C composite in long-term cycling.

diffusion coefficient D_{Li}^+ agrees with the Randle–Sevick equation below [27,28]:

$$I_p = (2.69 \times 10^5) n^{3/2} A D^{1/2} C^0 v^{1/2}$$

Here, I_p (A) is the peak current in the CV curves, n is the number of electrons transferred in the oxidation/reduction reaction, A (cm^2) is the surface area of the electrode, D ($cm^2\ s^{-1}$) is the diffusion coefficient of lithium ions, C^0 (mol cm^{-3}) is the concentration of lithium ions in $LiFe_{0.98}Ni_{0.02}PO_4$/C electrode, and v (V s^{-1}) is the scan rate of the potential during the CV measurement.

The calculated results show that the diffusion coefficient of lithium ions in $LiFe_{0.98}Ni_{0.02}PO_4$/C composite, D_{Li}^+, is 4.28×10^{-11} $cm^2\ s^{-1}$. By the same method, the diffusion coefficient for lithium ions in $LiFePO_4$/C-720 composite was calculated to be 2.10×10^{-11} $cm^2\ s^{-1}$, suggesting that doping with nickel benefits Li^+ insertion/extraction upon electrochemical cycling. By contrast, Liu et al. [28] measured D_{Li}^+ of a pure $LiFePO_4$ to be 2.485×10^{-11} $cm^2\ s^{-1}$ in Li_2SO_4 aqueous electrolyte, while Xie et al. [29] obtained a D_{Li}^+ on the order of 10^{-14} $cm^2\ s^{-1}$ in a mixture of ethylene carbonate/diethylene carbonate (1:1 in volume) with 1 mol L^{-1} of dissolved $LiClO_4$. Therefore, adding carbon and nickel dopant to $LiFePO_4$ obviously increases its D_{Li}^+ value.

In order to study the long-term cycling stability of the nickel doped composites, CVs of the $LiFe_{0.98}Ni_{0.02}PO_4$/C composite were collected for 1000 cycles at the scan rate of 5 mV s^{-1} in the potential range of 4.2–2.5 V, as shown in Fig. 7. The oxidation peaks in the 1st, 100th, 300th, 900th, and 1000th cycles appear at around 3.80, 3.77, 3.75, 3.85, and 3.85 V, respectively. The oxidation peak current is increased from 5.93 mA cm^{-2} (1st cycle) to 6.17 mA cm^{-2} (100th cycle), then decreased to 3.47 mA cm^{-2} (1000th cycle), indicating that the oxidation reaction of the composite gradually increased with cycling over the 1st to 100th cycles, and then decreased with cycling over the 100th cycle to 1000th cycle. The reduction peaks in the 1st, 100th, 300th, 900th, and 1000th cycle appear at around 3.29, 3.26, 3.14, 3.14, and 3.14 V, respectively. The reduction peak current gradually declined with cycling, indicating that the cycling stability decreased with cycling. The long-term CVs show that the cycling stability of the $LiFe_{0.98}Ni_{0.02}PO_4$/C composite gradually declines with cycling, however, the cycling stability is improved after 300 cycles.

3.4. Electrochemical impedance analysis

Fig. 8 shows the Nyquist plots and corresponding curve fitting results of the impedance spectra for the as-prepared nickel doped and un-doped composites, indicating that each spectrum

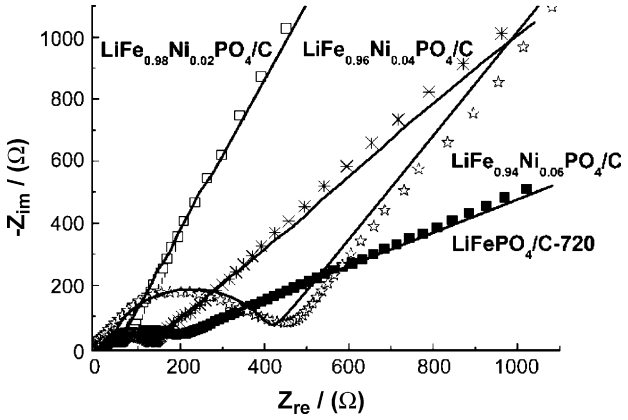

Fig. 8. Nyquist plots and corresponding curve fitting results of the impedance spectra for the as-prepared nickel doped and un-doped composites (symbols: experimental data, solid lines: fitting results for the impedance spectra).

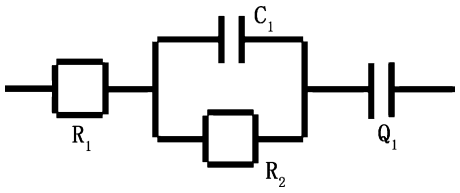

Fig. 9. Equivalent circuit of impedance spectra for the EIS of the as-prepared composites.

has one arc in the high-frequency zone and one sloping line in the low-frequency zone. The arc corresponds to charge-transfer resistance of particles in the electrolyte/sample interface [30,31]. The sloping line corresponds to the resistance of the individual cathode particles. Fig. 9 contains the equivalent circuit of the impedance spectra for the as-prepared composites, where R_{CT} and C_{DL} correspond to the charge-transfer resistance and double layer capacitance, respectively; R_p corresponds to the resistance of individual cathode particles (or the resistance between particles), Q_1 corresponds to the constant phase element. The fitted impedance data are listed in Table 2. When Q_1 substitutes for pure capacitance, $Z_{Q_1}^{-1} = C(j\omega)^n$. Here, Z_{Q_1} corresponds to the impedance of the pure capacitance, C corresponds to a constant independent of frequency, ω corresponds to angular frequency, $j=(-1)^{1/2}$. When n equals 0, 0.5, and 1, Z_{Q_1} corresponds to a pure resistance, a Warburg capacitance, and a pure capacitance, respectively.

Comparing the fitting parameters of the equivalent circuit in Table 2, it can be seen that the R_p and R_{CT} of the $LiFe_{0.98}Ni_{0.02}PO_4$/C composite are the lowest among all the nickel doped and un-doped composites. The charge-transfer resistance and cathode particle resistance of the $LiFe_{0.98}Ni_{0.02}PO_4$/C composite are obviously decreased compared to the other composites. Therefore, the electrochemical reaction of the $LiFe_{0.98}Ni_{0.02}PO_4$/C composite is carried out with low resistance.

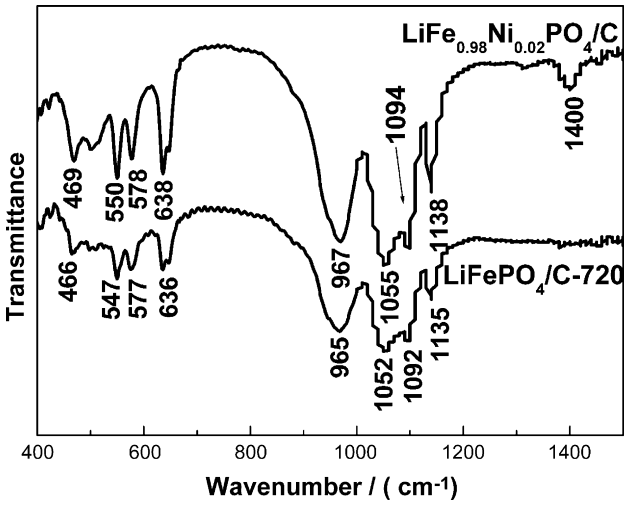

Fig. 10. FTIR spectra of the $LiFePO_4$/C-720 and $LiFe_{0.98}Ni_{0.02}PO_4$/C composites.

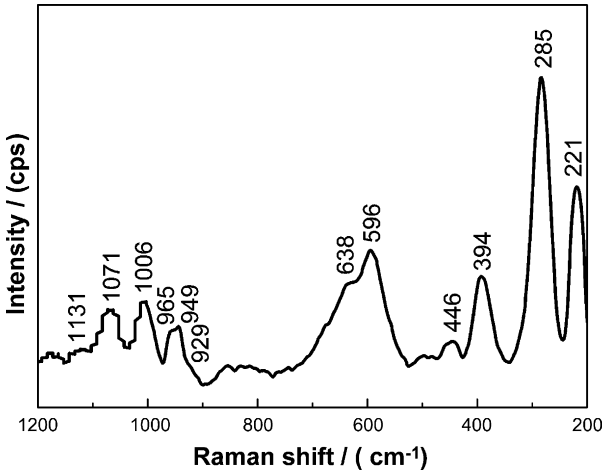

Fig. 11. Raman spectrum of the $LiFe_{0.98}Ni_{0.02}PO_4$ composite.

3.5. FTIR and Raman spectra of the samples

Fig. 10 contains the FTIR spectra of the $LiFePO_4$/C-720 and $LiFe_{0.98}Ni_{0.02}PO_4$/C composites, indicating that there are eight main FTIR peaks, located at 466, 547, 577, 636, 965, 1052, 1092, and 1135 cm^{-1}, respectively, in the FTIR spectrum of the $LiFePO_4$/C-720 composite; there are nine main FTIR peaks, located at 469, 550, 578, 638, 967, 1055, 1094, 1138, and 1400 cm^{-1}, respectively, in the FTIR spectrum of the $LiFe_{0.98}Ni_{0.02}PO_4$/C composite. Sundarayya et al. [32] and Bai et al. [33] measured the FTIR spectra of a $LiFePO_4$/C composite prepared by using a sol–gel process, with the results indicating that there are five peaks, located at 463, 547, 638, 966, and 1043 cm^{-1}, respectively. The FTIR peak located at 463 cm^{-1} corresponds to the bending vibration of the O—P—O and O=P—O groups, the peaks located at 547 and 638 cm^{-1} to the stretching vibration of the P—O—P groups, the peak located at 966 cm^{-1} to the

Table 2
Fitting parameters for the equivalent circuit of the corresponding as-prepared composites in Fig. 8.

Composites	$LiFePO_4$/C-720	$LiFe_{0.98}Ni_{0.02}PO_4$/C	$LiFe_{0.96}Ni_{0.04}PO_4$/C	$LiFe_{0.94}Ni_{0.06}PO_4$/C
R_p (Ω)	9.77	9.04	20.8	34.5
C_{DL} (μF)	0.442	1.79	0.617	0.253
R_{CT} (Ω)	103	40.0	85.2	354
Q_1 (10^{-5})	2.68×10^{-3}	7.16	0.399	0.273
n	0.313	0.754	0.503	0.658

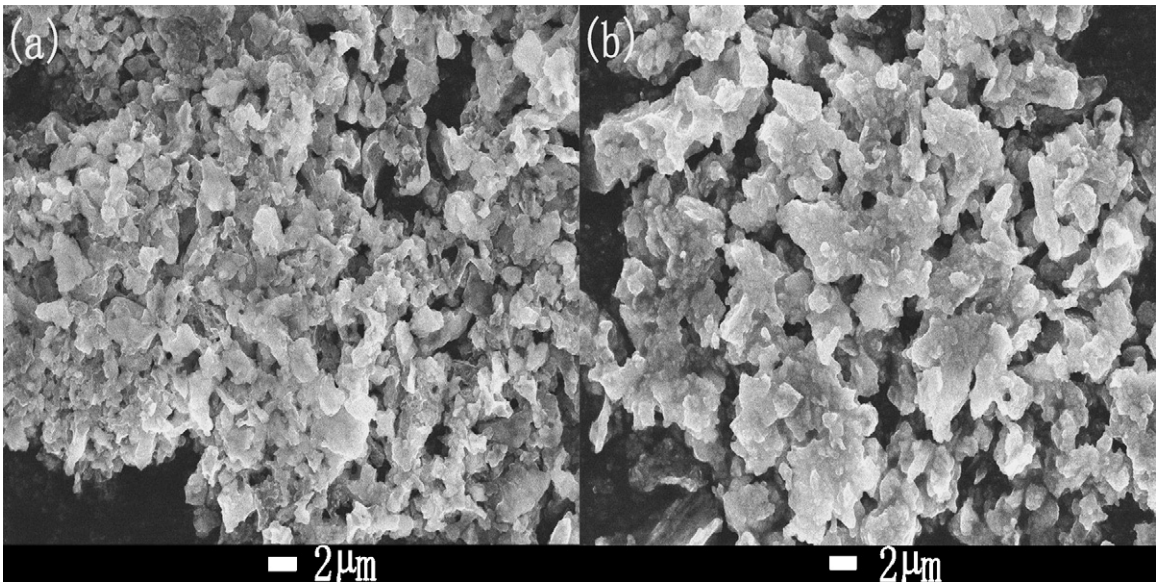

Fig. 12. Morphology of the $LiFePO_4$/C-720 (a) and $LiFe_{0.98}Ni_{0.02}PO_4$/C (b) composites.

bending vibration of the P—O—P groups, and the peak located at 1043 cm^{-1} to the vibration of the $(PO_4)^{3-}$ groups combined with metal ions. Compared to Sundarayya's experimental results [32], the nickel dopant enhances the P—O bond, indicating that the nickel dopant stabilizes the structure of the lithium iron phosphate.

Fig. 11 shows the Raman spectrum of the $LiFe_{0.98}Ni_{0.02}PO_4$ composite. Table 3 lists the Raman shifts of the $LiFe_{0.98}Ni_{0.02}PO_4$ and the corresponding Raman data in the literature [34–36]. The data in Table 3 and Fig. 11 indicate that the Raman peak (Rp) of the $LiFe_{0.98}Ni_{0.02}PO_4$ composite located around 1347 cm^{-1} can be identified as arising from carbon, while the Raman peaks (Rps) located around the ranges of 1311–965 and 596–446 cm^{-1} are identified as the vibration of the P—O bond, and the one located at 638 cm^{-1} is identified as the vibration of the FeO_x groups. The Raman peak is shifted to a higher wavenumber than in the literature [35,36] or in the $LiFePO_4$/C composite, indicating that the nickel dopant enhances the P—O and Fe—O bonds. This experimental result further confirms the results of the FTIR experiment and the charge–discharge cycling.

3.6. Morphology of the sample

Fig. 12 shows the morphology of the $LiFePO_4$/C-720 and $LiFe_{0.98}Ni_{0.02}PO_4$/C composites, indicating that the particle size of the $LiFePO_4$/C-720 composites is in the range of 1–4 μm, and that of the $LiFe_{0.98}Ni_{0.02}PO_4$/C composites is in the range of 2–6 μm. Fig. 13 shows the TEM (Fig. 13 (a)) and HRTEM (Fig. 13 (b)) images of the $LiFe_{0.98}Ni_{0.02}PO_4$/C composite, indicating that the micron-sized particles coated by a layer of carbon with the thickness about 2.8 nm. Therefore, the good electrochemical performance of the nickel doped composites is not associated with small particle size; instead, it is believed to result from nickel doping into the $LiFePO_4$ structure.

3.7. Ex situ XRD of the $LiFe_{0.98}Ni_{0.02}PO_4$/C electrode

To confirm that doping with nickel benefits the structure of $LiFePO_4$ upon cycling, we investigated the structure of the

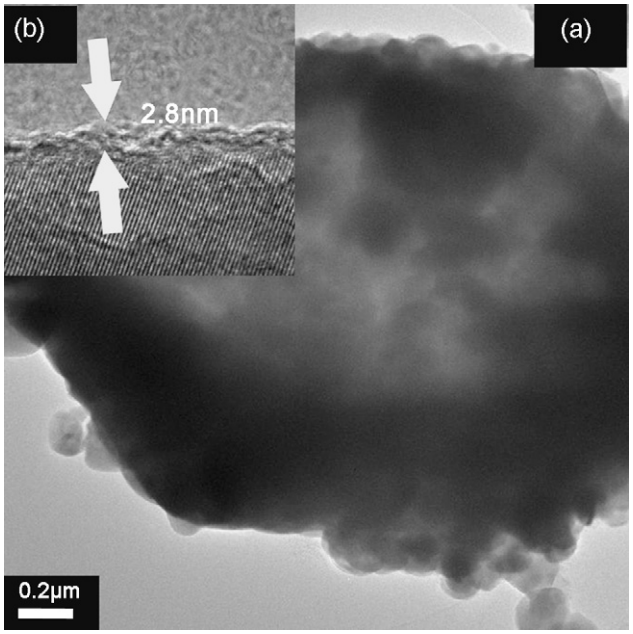

Fig. 13. TEM (a) and HRTEM (b) images of the $LiFe_{0.98}Ni_{0.02}PO_4$/C composite.

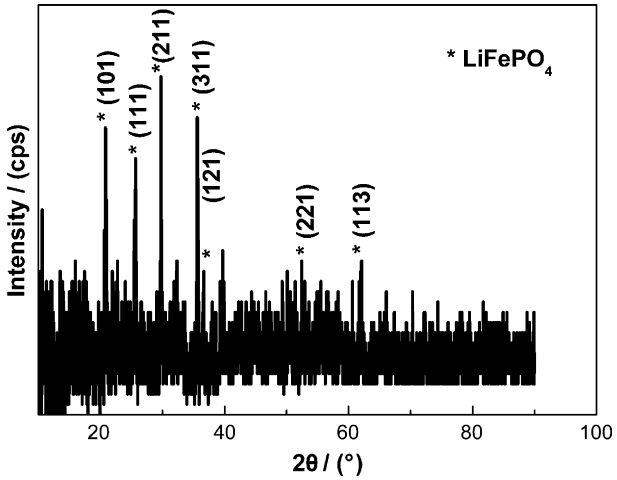

Fig. 14. XRD pattern of the $LiFe_{0.98}Ni_{0.02}PO_4$/C composite after 50 cycles.

Table 3
Rps (Raman peaks) of the $LiFePO_4$/C-720 and $LiFe_{0.98}Ni_{0.02}PO_4$/C composites, and corresponding Raman data from the literature [33–36].

$LiFePO_4$/C-720	Rp (cm^{-1})		1127 (m)	1070 (m)	995 (w)	952 (s)	911 (m)	882 (m)	629 (w)	590 (m)	422 (m)	303 (w)		
$LiFe_{0.98}Ni_{0.02}PO_4$/C	Rp (cm^{-1})	1347 (s)		1311 (w)	1006 (m)	965 (m)	949 (m)	929 (w)	638 (s)	596 (s)	446 (w)	394 (m)	285 (s)	221 (s)
Bai et al. [33]	Rp (cm^{-1})		1123	1069, 1081	998	951			623, 630	592, 573	445			
	Group		P—O						MO_6 or P—O	O—P—O				
	Vibration		Stretch							Bend				
Striebel et al. [34]	Rp (cm^{-1})	1583	1345		1087			650	605	530	418, 480			
	Group	C	C		LC			(w) FeO_x	FeO_x	FeO_x	FeO_x			
Bhuvaneswari et al. [35]	Rp (cm^{-1})				1051	988				581				
	Group				PO_4^{3-}	PO_4^{3-}				PO_4^{3-}				
	Vibration				Stretch					Stretch				
Konarova et al. [36]	Rp (cm^{-1})	1580	1339			945						276	214	
	Group	CNFs	CNFs			PO_4^{3-}						Fe_2O_3	Fe_2O_3	

In the table, (w) represents a weak peak, (m) represents a moderate peak, and (s) represents a strong peak. CNF refers to carbon nanofibers, C refers to graphite, and LC refers to lithium carbonate.

$LiFe_{0.98}Ni_{0.02}PO_4$/C electrode after 50 cycles at the 2 C rate. As shown in Fig. 14, all pattern peaks still belongs to the orthorhombic structure with space group *Pnmb*; no peak was found for any impurity, indicating that the structure of the $LiFe_{0.98}Ni_{0.02}PO_4$ composite is stable upon electrochemical cycling. Therefore, the nickel dopant can stabilize the orthorhombic structure of $LiFe_{0.98}Ni_{0.02}PO_4$ during charge/discharge cycling.

4. Conclusions

$LiFePO_4$/C and $LiFe_{1-x}Ni_xPO_4$/C ($x = 0$, 0.02, 0.04, and 0.06) were prepared using a solid-state sintering method. XRD analysis shows that all the nickel doped composites prepared at 720 °C can be indexed to a single phase having an orthorhombic olivine-type structure with space group *Pnmb*. When the discharge current is at the 30 C, 10 C, 2 C, 1 C, and 0.1 C rates, the discharge capacities of the $LiFe_{0.98}Ni_{0.02}PO_4$/C are 35, 70, 121, 127, and 142 mAh g^{-1} in the 1st cycle, and 35, 67, 108, 119, and 138 mAh g^{-1} in the 50th cycle, respectively. Comparing the nickel doped and un-doped composites, the nickel doping extends the length of the discharge plateau at high voltage. The diffusion coefficient of lithium ions in $LiFe_{0.98}Ni_{0.02}PO_4$/C composite, $D_{Li}{}^+$, is 4.28×10^{-11} cm^2 s^{-1}. The EIS analysis shows that the charge-transfer resistance and the cathode particle resistance of the $LiFe_{0.98}Ni_{0.02}PO_4$/C composite are obviously decreased in all the as-prepared composites. The nickel doped lithium iron phosphate has a stable structure with an optimal size of the cell volume, and the diffusion of lithium in the $LiFe_{0.98}Ni_{0.02}PO_4$/C composite is easier than in the un-doped sample. Therefore, the nickel dopant improves the electrochemical performance of lithium iron phosphate.

Acknowledgements

Financial support from the Education Ministry of China (Grant No. 03065), the Natural Science Foundation of Fujian Province, China (Grant No. 2008J0144), and the Fujian Provincial Development and Reform Commission (Grant Ref. Mingfagai Gaoji [2008]794 Hao) is gratefully acknowledged. Dr. X.K. Huang helped to correct some grammatical errors.

References

[1] A.K. Padhi, K.S. Najundaswamy, J.B. Goodenough, J. Electrochem. Soc. 144 (1997) 1188.
[2] S. Yang, Y. Song, P.Y. Zavalij, M.S. Whittingham, Electrochem. Commun. 3 (2002) 239.
[3] D.D. MacNeil, Z. Lu, Z. Chen, J.R. Dahn, J. Power Sources 108 (2002) 8.
[4] Y.-D. Cho, G.T.-K. Fey, H.-M. Kao, J. Power Sources 189 (2009) 256.
[5] S.J. Kwon, C.W. Kim, W.T. Jeong, K.S. Lee, J. Power Sources 137 (2004) 93.
[6] C. Delmas, M. Maccario, L. Croguennec, F.L. Cras, F. Weill, Nat. Mater. 7 (2008) 597.
[7] S.-Y. Chung, J.T. Bloking, Y.-M. Chiang, Nat. Mater. 1 (2002) 123.
[8] M.-S. Wu, M.-J. Wang, J.-J. Jow, W.-D. Yang, C.-Y. Hsieh, H.-M. Tsai, J. Power Sources 185 (2008) 1420.
[9] G.X. Wang, S.L. Bewlay, K. Konstantinov, H.K. Liu, S.X. Dou, J.-H. Ahn, Electrochim. Acta 50 (2004) 443.
[10] J.B. Heo, S.B. Lee, S.H. Cho, J. Kim, S.H. Park, Y.S. Lee, Mater. Lett. 63 (2009) 581.
[11] W.-S. Yoon, K.Y. Chung, K.-W. Nam, J. McBreen, D. Wang, X. Huang, H. Li, L. Chen, X.-Q. Yang, J. Power Sources 183 (2008) 427.
[12] H.C. Shin, S.B. Park, H. Jang, K.Y. Chung, W. Cho, C.S. Kim, B.W. Cho, Electrochim. Acta 53 (2008) 7946.
[13] H.-H. Chang, C.-C. Chang, C.-Y. Su, H.-C. Wu, M.-H. Yang, N.-L. Wu, J. Power Sources 185 (2008) 466.
[14] X.J. Chen, G.S. Cao, X.B. Zhao, J.P. Tu, T.J. Zhu, J. Alloys Compd. 463 (2008) 385.
[15] J. Xu, G. Chen, Y.-J. Teng, B. Zhang, Solid State Commun. 147 (2008) 414.
[16] T. Shiratsuchi, S. Okada, T. Doi, J. Yamaki, Electrochim. Acta 54 (2009) 3145.
[17] J.A. Dean, Lange's Chemistry Handbook, 15th ed., McGraw-Hill, Inc., 1999, 4.3.
[18] H.X. Zhang, Q.S. Tong, S.Y. Lin, Inorg. Chem. Industry 36 (2004) 26.
[19] Q.S. Tong, Y. Yang, J.C. Shi, J.M. Yan, L.Q. Zheng, J. Electrochem. Soc. 154 (2007) A656.
[20] J.-K. Kim, J.-W. Choi, G.S. Chauhan, J.-H. Ahn, G.-C. Hwang, J.-B. Choi, H.-J. Ahn, Electrochim. Acta 53 (2008) 8258.
[21] A. Nytén, J.O. Thomas, Solid State Ionics 177 (2006) 1327.

[22] D. Wang, Z. Wang, X. Huang, L. Chen, J. Power Sources 146 (2005) 580.
[23] D. Shanmukaraj, G.X. Wang, R. Murugan, H.K. Liu, Mater. Sci. Eng. B 149 (2008) 93.
[24] D. Cheng, X. Xi, Y. Li, W. Qiu, P. Chen, Min. Metall. Eng. (China) 28 (2008) 91.
[25] D. Wang, H. Li, S. Shi, X. Huang, L. Chen, Electrochim. Acta 50 (2005) 2955.
[26] B. Jin, E.M. Jin, K.-H. Park, H.-B. Gu, Electrochem. Commun. 10 (2008) 1537.
[27] P.P. Prosini, M. Lisi, D. Zane, M. Pasquali, Solid State Ionics 148 (2002) 45.
[28] Y. Liu, C. Mi, C. Yuan, X. Zhang, J. Electroanal. Chem. 628 (2009) 73.
[29] J. Xie, N. Imanishi, T. Zhang, A. Hirano, Y. Takeda, O. Yamamoto, Electrochim. Acta 54 (2009) 4631.
[30] F. Gao, Z.Y. Tang, Electrochim. Acta 53 (2008) 5071.
[31] K. Shizuk, S. Takano, K. Okahara, J. Power Sources 174 (2007) 1074.
[32] Y. Sundarayya, K.C. Kumara, C.S. Sunandana, Mater. Res. Bull. 42 (2007) 1942.
[33] Y. Bai, F. Wu, C. Wu, Chin. J. Light Scattering 15 (2004) 231.
[34] K. Strieber, J. Shim, A. Sierra, H. Yang, X. Song, R. Kentucky, K. McCarthy, J. Power Sources 146 (2005) 33.
[35] M.S. Bhuvaneswari, N.N. Bramnik, D. Ensling, H.E. Jaegermann, J. Power Sources 180 (2008) 553.
[36] M. Konarova, I. Taniguchi, Mater. Res. Bull. 43 (2008) 3305.